Simulating rhizodeposition patterns around growing and exuding root systems

Magdalena Landl*[1], Adrian Haupenthal[1], Daniel Leitner[2], Eva Kroener[1,3], Doris Vetterlein[4,5], Roland Bol[1], Harry Vereecken[1], Jan Vanderborght[1], and Andrea Schnepf[1]

[1]Forschungszentrum Juelich GmbH, Agrosphere (IBG-3), Juelich, Germany
[2]Simulationswerkstatt, Ortmayrstrasse 20, A-4060 Leonding, Austria
[3]Institute of Crop Science and Resource Conservation (INRES), Soil Science and Soil Ecology, University Bonn, Bonn, Germany
[4]Department Soil System Sciences, Helmholtz Centre for Environmental Research-UFZ, Halle/Saale, Germany
[5]Martin-Luther-University Halle-Wittenberg; Institute of Agricultural and Nutritional Sciences, Halle/Saale, Germany

*Correspondence:
Magdalena Landl
Forschungszentrum Juelich GmbH, Agrosphere (IBG-3)
D- 52428 Juelich, Germany
Tel.: +49 2461 61 8835
Email: m.landl@fz-juelich.de

1 Abstract

In this study, we developed a novel model approach to compute the spatio-temporal distribution patterns of rhizodeposits around growing root systems in three dimensions. Root systems were generated using the root architecture model CPlantBox. The concentration of rhizodeposits at a given location in the soil domain was computed analytically. To simulate the spread of rhizodeposits in the soil, we considered rhizodeposit release from the roots, rhizodeposit diffusion into the soil, rhizodeposit sorption to soil particles, and rhizodeposit degradation by microorganisms. To demonstrate the capabilities of our new model approach, we performed simulations for the two example rhizodeposits mucilage and citrate and the two example root systems *Vicia faba* and *Zea mays*. The rhizodeposition model was parameterized using values from the literature. Our simulations showed that the rhizosphere soil volume with rhizodeposit concentrations above a defined threshold value (i.e., the rhizodeposit hotspot volume), exhibited a maximum at intermediate root growth rates. Root branching allowed the rhizospheres of individual roots to overlap, resulting in a greater volume of rhizodeposit hotspots. This was particularly important in the case of citrate, where overlap of rhizodeposition zones accounted for more than half of the total rhizodeposit hotspot volumes. The rhizodeposit hotspot volume around the tap root system *Vicia faba* was shown to be much larger than around the fibrous root system *Zea mays*. Coupling a root architecture

model with a rhizodeposition model allowed us to get a better understanding of the influence of root architecture as well as rhizodeposit properties on the evolution of the spatio-temporal distribution patterns of rhizodeposits around growing root systems.

2 Introduction

The rhizosphere is defined as the small soil volume around the roots, in which plant roots interact with the soil and thereby alter its physical, chemical and biological properties (Hinsinger et al., 2009). One important rhizosphere process is rhizodeposition, which is defined as the free or passive release of organic compounds by the root, including water-soluble exudates, secretion of insoluble materials and also enzymes such as acid phosphatase, and release of dead root cells (Cheng and Gershenson, 2007). Rhizodeposition affects the ability of plant roots to extract water and nutrients from the soil, which is particularly important when resources are scarce (Hinsinger et al., 2009). Knowledge about the spatial distribution of rhizodeposits in the soil domain is thus crucial (Darrah, 1991).

There are only limited possibilities to directly measure the spatio-temporal distribution patterns of rhizodeposits around a root system. Holz et al. (2018a) used infrared spectroscopy to determine the spatial distribution of mucilage in the rhizosphere. This method allowed them to visualize the axial and radial gradients of mucilage concentration around a single root at a given point in time; information on the temporally dynamic distribution of mucilage is, however, lacking. Under the assumption of a constant ratio between rhizodeposited carbon and root carbon, Pausch et al. (2013) quantified rhizodeposition at the field scale. This approach enabled them to estimate the total amount of rhizodeposition of an entire root system over a defined period of time, however, it does not give any information about the spatial distribution patterns of rhizodeposits.

Simulation models can contribute to better understand the processes leading to rhizodeposition and its spatial and temporal distribution. Such models that describe the distribution of rhizodeposits in the soil domain need to take into account the following processes: the rhizodeposit release by the roots, the diffusion of rhizodeposits into the soil domain, and the decomposition of rhizodeposits by microorganisms (Kirk, 1999). For some organic compounds such as citrate, also sorption to the soil particles plays an important role (Oburger et al., 2011). A common approach to dynamically compute rhizodeposition patterns in the soil domain is the use of the diffusion-reaction equation. To our knowledge, however, this approach has so far only been applied at the single root scale (Carminati et al., 2016a; Holz et al., 2018b; Kirk, 1999) or extrapolated from the single root scale to the root system scale, neglecting differences in rhizodeposition patterns along the root axis (Schnepf et al., 2012). Fletcher et al. (2020) used a citrate-phosphate solubilization model to compute the spatio-temporal distribution of citrate concentrations around root systems in three dimensions. Their approach is, however, limited to very small root systems ($\leq 8\,cm$ rooting depth) due to

computational limitations.

Various studies have shown the importance of the effect of root architecture on the amount and distribution of rhizodeposits (Hodge et al., 2009; Lynch, 1995; Lynch, Ho, et al., 2005; Manschadi et al., 2014). On the one hand, root architecture controls the amount of rhizodeposit release by the number of root tips (Nielsen et al., 1994). On the other hand, root branching and root growth rate determine whether rhizodeposit release zones can overlap, thereby creating patches of high rhizodeposit concentration, which may facilitate water and nutrient uptake (De Parseval et al., 2017; Holz et al., 2018b).

Rhizodeposition was shown to affect rhizosphere processes such as water and nutrient acquisition only if its concentration exceeds a defined threshold value (i.e., the rhizodeposit hotspot concentration) (Ahmed et al., 2016; Fletcher et al., 2019; Gerke, 2015). However, it is not yet clear when and where around the growing root system such zones of rhizodeposit hotspot concentrations arise, how they are distributed, and what proportion of the total concentration volume they represent. Not only the location of a rhizodeposit hotspot, but also the distance and connectivity to the nearest hotspot and its duration can be a relevant factor controlling soil microbial diversity and microbial activities (Carson et al., 2010). Certain bacteria respond to threats or nutrient availability even when detected from certain distances: volatile organic compounds can provide information over larger distances and diffusible compounds over smaller distances (Schulz-Bohm et al., 2017; Westhoff et al., 2017).

The aim of this study was to couple a root architecture model that simulates the development of a 3D root system with a rhizodeposition model that simulates the transport of rhizodeposits to investigate the spatio-temporal distribution patterns of rhizodeposits in the soil and to evaluate the influence of root architecture on the generated patterns. For our simulations, we selected the two rhizodeposits citrate and mucilage, which have very distinct properties. In a first scenario, we simulated rhizodeposition by a single growing root. This scenario was used to evaluate the impact of the different rhizodeposit properties such as the rhizodeposit release rate, the sorption to soil particles as well as rhizodeposit decomposition and diffusion on the axial and radial distribution patterns of rhizodeposits around the root. In a second scenario, we investigated the impact of the two root architectural traits 'root growth rate' and 'number of root tips' on the rhizodeposition patterns around a growing single root respectively a simple herringbone root system. In a third scenario, we simulated rhizodeposition around entire growing root systems. For these simulations, we selected the tap and fibrous root systems of *Vicia faba* and *Zea mays*. This scenario was used to evaluate the impact of the different root architectures on the spatio-temporal distribution patterns of the rhizodeposits. For the root system of *Vicia faba*, we investigated for how long and where in the soil domain the rhizodeposit concentrations were above a critical threshold value and evaluated the importance of root branching and overlap of rhizodeposit release zones for the emergence of such rhizodeposit hotspots. Furthermore, we studied how the amount of soil volumes at various distances around rhizodeposit hotspots evolves over time.

3 Material and Methods

3.1 Model development

To simulate rhizodeposition patterns around growing and exuding root systems, we considered roots as point or line sources. The potential impact of the root diameter on the concentration of rhizodeposits was thus neglected. Making these assumptions, the concentration of rhizodeposits at a given location in the soil domain can be computed analytically. All equations and assumptions underlying our coupled model approach are explained in the following.

3.1.1 Root growth model

All root systems were created with the root architecture model CPlantBox, which is described in detail in Schnepf et al. (2018) and Zhou et al. (2020). CPlantBox is a generic model, which allows simulating diverse root architectures of any monocotyledonous and dicotyledonous plant. It distinguishes between different root types, i.e. tap root, basal roots and lateral roots of different order. Each root type is defined by a certain set of parameters that determine its evolution over time. CPlantBox is programmed in C++, but includes a Python binding that allows simplified scripting.

3.1.2 Rhizodeposition model - theory

For each growing root, we solve the diffusion-reaction equation (Jacques et al., 2018) in an infinite domain,

$$\theta R \frac{\partial c}{\partial t} + \nabla \cdot (-D\theta \nabla c) = -\theta k c + f(\mathbf{x}, t) \qquad \text{for } t > 0,\ \mathbf{x} \in \mathbb{R}^3, \tag{1}$$

$$c(\mathbf{x}, 0) = 0 \tag{2}$$

where θ is the volumetric water content ($cm^3\, cm^{-3}$), R is the retardation coefficient ($cm^3\, cm^{-3}$), c is the rhizodeposit concentration in the soil ($\mu g\, cm^{-3}$), $D = D_l \tau$ is the effective diffusion coefficient ($cm^2\, d^{-1}$), D_l is the molecular diffusion coefficient in water ($cm^2\, d^{-1}$), τ is the impedance factor ($-$), k is the linear first order decomposition rate constant (d^{-1}), f is the source term that describes the release of rhizodeposits by the root at position $\mathbf{x}$ and time t.

We consider two cases of rhizodeposition: In the first case, rhizodeposition occurs at the root tip only and the root is thus considered as a moving point source; in the second case, rhizodeposition occurs over a given root length l behind the tip and the root is a moving line source. For these two cases, the source term f is defined as

$$f(\mathbf{x}, t)_{point} = Q_p \delta(\mathbf{x} - \mathbf{x}_{tip}(t)) \tag{3}$$

$$f(\mathbf{x}, t)_{line} = \int_0^{min(l_r, l)} Q_l \delta(\mathbf{x} - \mathbf{x}(l', t)) dl' \tag{4}$$

where Q_p ($\mu g\, d^{-1}$) and Q_l ($\mu g\, d^{-1}\, cm^{-1}$) are the rhizodeposit release rates of the point and line sources, $\mathbf{x}_{tip}(t) = (x_{tip}, y_{tip}, z_{tip})$ is the position of root tip at time t, l_r is the arc length of the exuding root segment (cm), $\mathbf{x}(l', t)$ is the position at an arc length of l' behind the position of the root tip at time t, and $\delta(\mathbf{x})$ (cm^{-3}) is the Dirac function.

The analytical solutions to these moving point and moving line source problems have been derived by Carslaw and Jaeger (1959), Bear and Cheng (2010), Wilson and Miller (1978):

$$c(\mathbf{x}, t) = \int_0^{age_r(t)} \frac{Q_p R^{1/2}}{8\theta\sqrt{\pi^3 D^3 t'^3}} exp(-R\frac{(\mathbf{x} - \mathbf{x}_{tip}(age_r(t) - t'))^2}{4Dt'} - \frac{k}{R}t')dt' \tag{5}$$

$$c(\mathbf{x}, t) = \int_0^{min(l_r, l)} \int_0^{age_r(t)} \frac{Q_l R^{1/2}}{8\theta\sqrt{\pi^3 D^3 t'^3}} exp(-R\frac{(\mathbf{x} - \mathbf{x}(l', age_r(t) - t'))^2}{4Dt'} - \frac{k}{R}t')dt'dl', \tag{6}$$

where $age_r(t)$ is the age of an individual root at time t (d).

We assume that rhizodeposition stops when the root stops growing. The rhizodeposits, which are already present in the soil, however, continue to diffuse and decompose. Thus, after the root stopped growing, we need to solve:

$$\theta R\frac{\partial c}{\partial t} + \nabla \cdot (-D\theta\nabla c) = -\theta kc \qquad \text{for } t > t_{stop},\ \mathbf{x} \in \mathbb{R}^3, \tag{7}$$

$$c(\mathbf{x}, t_{stop}) = g(\mathbf{x}, t_{stop}), \tag{8}$$

where $g(\mathbf{x}, t_{stop})$ is the solution concentration ($\mu g\, cm^{-3}$) at time t_{stop} (d). The analytical solution of the problem with first-order reaction term given by equations (7) and (8) can be derived from the general solution of the homogeneous initial value problem (Evans, 1998) by making use of the transformation $c' = c \times exp(-k/R \times t)$ (Crank, 1979), where c' is the general solution of the homogeneous problem (Evans, 1998):

$$c(\mathbf{x}, t) = \int_{\mathbb{R}^3} \frac{R^{3/2} g(\mathbf{y}, t_{stop})}{(4D\pi(t - t_{stop}))^{3/2}} exp\left(-R\frac{(\mathbf{x} - \mathbf{y})^2}{4D(t - t_{stop})} - \frac{k(t - t_{stop})}{R}\right) d\mathbf{y} \tag{9}$$

The solution concentration around an entire root system was computed by adding up the concentrations around individual roots, making use of the superposition principle. Thus, the total solution concentration c_T around N roots is given by:

$$c_T(\mathbf{x}, t) = \sum_i^N c_i(\mathbf{x}, t) \tag{10}$$

3.1.3 Rhizodeposition model - application

The rhizodeposition model was implemented as an additional module in the root architecture model CPlantBox. The analytical solutions presented in equations (5) and (6) were solved numerically using the Gauss-Legendre quadrature, which we derived from the open source library for C/C++ provided by Pavel Holoborodko (http://www.holoborodko.com/pavel/). This library was used within the C++ code of CPlantBox and introduced into its Python binding so that we could compute the rhizodeposit distribution around a simulated root architecture. The analytical solution for the moving point source (equation (5)) was solved using the function 'gauss legendre', while the analytical solution for the moving line source (equation (6)) was solved using the function 'gauss legendre 2D cube' with 10 integration points per $1\,cm$ root length. The volume integral in equation (9) was solved by trapezoidal rule over a regular cubic grid of $1\,mm$ edge length, and the integral was scaled in order to achieve mass balance for diffusion.

To reduce computational time, equations (5) and (6) were not evaluated for the entire soil domain, but only within a specified maximum influence radius around each root within which the rhizodeposit concentrations were significantly different from zero. This maximum influence radius was set to $0.6\,cm$ for citrate and to $0.4\,cm$ for mucilage, which was a rough estimation of the diffusion length. Since we used analytical solutions, the rhizodeposit concentrations had to be calculated individually around each root before they were added to get the concentration around the whole root system. To reduce computational time, we calculated the rhizodeposit concentrations around the individual roots of a root system in parallel using the multiprocessing package available in Python. In addition, it was necessary to run our model individually for each time step for which an output was needed. We ran all simulations on the Linux cluster of IBG-3 at the Research Center Juelich, which allowed us to run several model runs in parallel. The rhizodeposition model with the code used in this study is publicly available at https://github.com/Plant-Root-Soil-Interactions-Modelling/CPlantBox/tree/pub_landl_2021.

3.2 Scenario setup and model parameterization

In a first scenario, we simulated rhizodeposition by a single growing root. This scenario was used to investigate the radial and axial distribution of rhizodeposits around the root. In this scenario, the root was assumed to grow straight downwards at a constant growth rate of $1\,cm\,d^{-1}$ until a root length of $10\,cm$ was reached. The root then stopped growing. Rhizodeposition was computed for the two rhizodeposits citrate and mucilage, which have very distinct properties. We used mucilage and citrate rhizodeposit release rates of *Vicia faba*. The rhizodeposit release rate is lower for citrate than for mucilage. The diffusion coefficient and the decomposition rate, in contrast, are higher for citrate than for mucilage. Furthermore, citrate is known to be sorbed to the soil particles (Oburger et al., 2011), while mucilage that is in contact with free water is not

(Sealey et al., 1995). While citrate is exuded from the root apex over a length of approximately 5 cm (Pineros et al., 2002), mucilage was shown to be deposited from an area of only a few mm^2 right at the tip of the root (Iijima et al., 2003). All rhizodeposit properties were derived from literature and are presented in Table 1.

In a second scenario, we evaluated the impact of the two root architectural traits 'root growth rate' and 'branching density' on the rhizodeposition patterns around a growing single root respectively a simple herringbone root system. We thereby used four different constant root growth rates ($0.1\,cm\,d^{-1}$, $0.5\,cm\,d^{-1}$, $1\,cm\,d^{-1}$, $1.5\,cm\,d^{-1}$) respectively two different branching densities ($2\,cm^{-1}$ and $1\,cm^{-1}$). Citrate and mucilage rhizodeposit release rates were parameterized for *Vicia faba* using values from the literature (Table 1).

In a third scenario we simulated rhizodeposition by entire growing root systems that were generated with CPlantBox to investigate the impact of different root architectures as well as the characteristics of different plants on the spatio-temporal distribution patterns of rhizodeposits. We chose the model plants *Vicia faba* and *Zea mays* with their contrasting tap and fibrous root systems. Root architecture parameters were obtained from µCT images of *Vicia faba* and *Zea mays* plants that were grown in a lab experiment (Gao et al., 2019). The root systems shown on the µCT images were thereby manually reconstructed in a three-dimensional virtual reality system (Stingaciu et al., 2013) and saved as RSML files (Lobet et al., 2015). These RSML files were then used to derive the required input parameters of CPlantBox with the help of a home-grown python code. All input parameters are presented in the Appendix. The rhizodeposit release rates of citrate and mucilage were adapted to *Vicia faba* and *Zea mays* using values from the literature and are presented in Table 1. The simulation time was set to 21 days, which is a typical time frame of the lab experiments that were used to image the plant root systems. Simulation outputs were generated in daily time steps. The size of the soil domain was $20 \times 20 \times 45\,cm^3$ for *Vicia faba* and $40 \times 40 \times 35\,cm^3$ for *Zea mays*. In all simulation scenarios, the resolution of the soil domain was set to $1\,mm$ and we used a constant soil water content of $0.3\,cm^3\,cm^{-3}$.

Table 1: Parameters used in the rhizodeposition model

Parameter	Symbol	Value		Unit	Source
		Mucilage	Citrate		
Diffusion coefficient in water	D_l	3.46E-03	0.57	$cm^2\,d^{-1}$	Watt et al. (2006)
Diffusion impedance factor	τ	0.3	0.3	-	Olesen et al. (2001)
Retardation coefficient	R	1	16.7	$(cm^3\,cm^{-3})$	Oburger et al. (2011), $R = \frac{b}{\theta}$, b is the buffer power $(-)$
Rhizodeposit release rate, *Vicia faba*	Q	33.38	18.4	$\mu g\,d^{-1}\,root\,tip^{-1}$/ $\mu g\,d^{-1}\,cm\,root^{-1}$	Zickenrott et al. (2016), Rangel et al. (2010)
Rhizodeposit release rate, *Zea mays*	Q	5.27	3.7	$\mu g\,d^{-1}\,root\,tip^{-1}$/ $\mu g\,d^{-1}\,cm\,root^{-1}$	Zickenrott et al. (2016), Pineros et al. (2002)
Decomposition rate	k	0.22	1.42	d^{-1}	Nguyen et al. (2008), Kirk (1999)
Deposition length behind the root tip	l	-	5	cm	Iijima et al. (2003), Pineros et al. (2002)

3.2.1 Rhizodeposit hotspot analysis

Rhizodeposit hotspots are defined as the soil volumes around the root in which the concentration of rhizodeposits is above a critical threshold value and therefore significantly influences specific rhizosphere processes. We defined these threshold values for citrate and mucilage using values from the literature. Gerke (2015) reported that a minimum total carboxylate concentration of $5\,\mu mol\,g^{-1}$ soil leads to enhanced phosphorus mobilization. Assuming that citrate accounts for about 25 % of the total carboxylate concentration (Lyu et al., 2016) and using the soil buffer power as the ratio between the total rhizodeposit concentration and the soil solution rhizodeposit concentration (Nye, 1966), this corresponds to a threshold citrate concentration of $58\,\mu g\,cm^{-3}$ soil solution at an assumed bulk density of $1.2\,g\,cm^{-3}$. In a modelling study based on experimental measurements, Carminati et al. (2016a) investigated the effect of mucilage on rhizosphere hydraulic properties and transpiration as a function of mucilage concentration. For a sandy soil, they observed a measurable effect of mucilage on soil water retention at a minimum mucilage concentration of $0.33\,mg\,g^{-1}$ dry soil, which corresponds to a threshold mucilage concentration of $1300\,\mu g\,cm^{-3}$ soil solution at an assumed bulk density of $1.2\,g\,cm^{-3}$. It was shown that not only fresh mucilage, but also mucilage derivatives that are produced during the process of decomposition can have an impact on soil hydraulic properties (Carminati and Vetterlein, 2013; Or et al., 2007). To date, however, it is not clear how mucilage derivatives affect soil water dynamics (Benard et al., 2019). In this study, degraded mucilage is neglected and only the concentration of fresh mucilage is taken into account.

To compare hotspot volumes of root systems that differ in architecture or age, we normalized them with the root length and with the minimum soil volume that contains 99 % of the total rhizodeposit mass that is currently present in the soil domain. These relative hotspot volumes are further on called length-normalized and volume-normalized rhizodeposit hotspot volumes. While the length-normalized hotspot volume is a measure of the efficiency of the root architecture, the volume-normalized rhizodeposit hotspot volume can be regarded as a measure of the efficiency of rhizodeposition.

The duration of an individual rhizodeposit hotspot at a specific location in the soil domain is not constant, but varies depending on different dynamic processes such as the diffusion and decomposition rate, the sorption to soil particles, the deposition length behind the root tip and the root architecture, which may cause rhizodeposit overlap. We therefore also investigated the lifetime of rhizodeposit hotspots within the soil domain.

To quantify the amount of soil volumes at various distances around hotspots and how these quantities evolve over time, we applied the 3D ImageJ Suite (Ollion et al., 2013) plugin of Fiji (Schindelin et al., 2012) to calculate the Euclidean 3D distance maps from the nearest hotpots at various days of root growth and provide the histograms of the distance maps.

4 Results

4.1 Scenario I: Rhizodeposition by a single growing root

Fig. 1 shows the concentration profiles of citrate and mucilage around a growing and exuding single root after a defined time period. After 10 days, the root reaches its maximum length of 10 cm and both root growth and rhizodeposition stop. Diffusion and decomposition of the rhizodeposits continue until the end of the simulation. For both citrate and mucilage, the concentrations are thus much higher after 10 days (Fig.1 (I)) than after 15 days (Fig.1 (II)) of simulation due to the ongoing decomposition of the rhizodeposits. The progressive diffusion furthermore leads to a larger extent of the radial profiles after 15 days compared to 10 days and also at position 2 (15 cm behind the root tip) compared to position 1 (1.5 cm behind the root tip). In general, concentrations of mucilage are higher than concentrations of citrate due to the differences in rhizodeposit properties. The peak concentration of mucilage is located at a distance of 1 cm behind the root tip, while citrate concentrations are highest 5 cm behind the root tip. This difference is caused by the differences in the deposition lengths (Table 1, Fig.1 (a)). The radial extension of the concentration from the root axis is larger for citrate than for mucilage due to the larger ratio of the effective diffusion coefficient and the retardation factor (Fig.1 (b,c)). The rhizodeposit hotspot concentrations extend over a length of 5.3 cm and 2.2 cm along the root axis for citrate and mucilage, respectively, while the root is still growing (Fig.1 Ia). The maximum radial extent of the rhizodeposit hotspot concentration is 1 mm and 0.5 mm for citrate and mucilage, respectively, while the root is still growing (Fig.1 Ib, c).

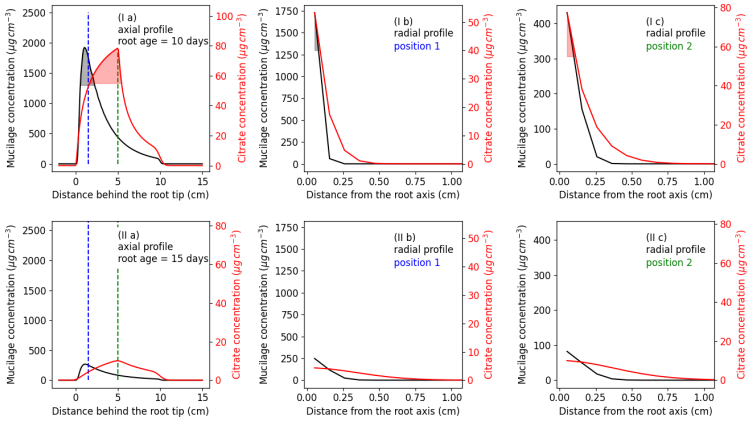

Figure 1: Concentration profiles of mucilage and citrate after (I) 10 and (II) 15 days: along the root axis (a) and radially from the root axis at a distance of $1.5\,cm$ (position 1) (b) and $15\,cm$ (position 2) (c) from the root tip; the shaded areas denote the part of the profiles where the concentrations are above the threshold values

4.2 Scenario II: Impact of root architectural traits on the rhizodeposition patterns around a single growing root

4.2.1 Impact of root growth rate

Considering that rhizodeposits are released from the growing tip in the case of mucilage respectively from a small zone behind the growing tip in the case of citrate, changes in root elongation rate have a strong impact on the distribution of rhizodeposits in the soil. In figures 2 and 3 the concentrations of mucilage and citrate around a single straight root that elongates for 10 days at different constant growth rates are shown. A larger growth rate obviously leads to a larger soil volume containing rhizodeposits at a lower concentration. In black, we depicted the volume of rhizodeposit hotspots for both citrate and mucilage. Interestingly, the largest rhizodeposit hotspot volume was found for the second lowest root growth rate of $0.5\,cm\,d^{-1}$ for citrate and for the second highest root growth rate of $1\,cm\,d^{-1}$ for mucilage. This can be explained by the opposite effect of the growth rate on the concentration where exudation takes place, which increases with decreasing growth rate, and of the soil volume containing rhizodeposits, which increases with increasing growth rate.

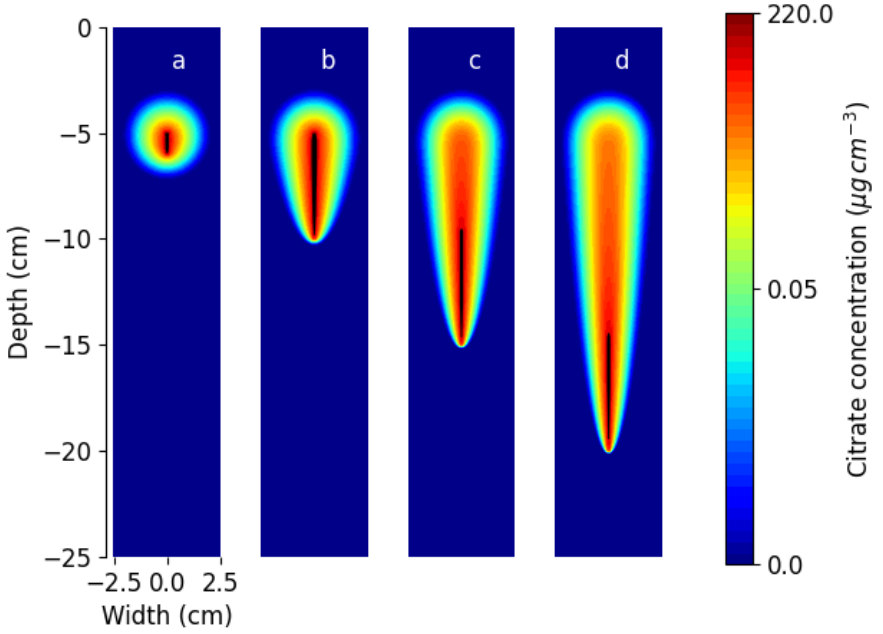

Figure 2: Concentration of citrate deposits around a single root after 10 days of growth at a constant growth rate of (a) $0.1\, cm\, d^{-1}$, (b) $0.5\, cm\, d^{-1}$, (c) $1\, cm\, d^{-1}$, (d) $1.5\, cm\, d^{-1}$; the black patches denote the hotspot volume; note that the colors are in logarithmic scale

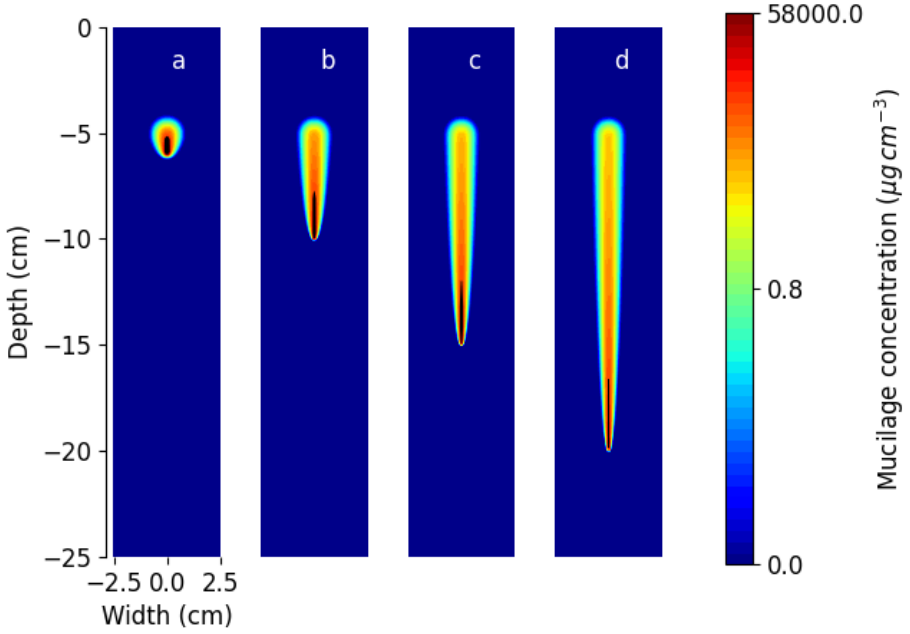

Figure 3: Concentration of mucilage deposits around a single root after 10 days of growth at a constant growth rate of (a) $0.1\,cm\,d^{-1}$, (b) $0.5\,cm\,d^{-1}$, (c) $1\,cm\,d^{-1}$, (d) $1.5\,cm\,d^{-1}$; the black patches denote the hotspot volume; note that the colors are in logarithmic scale

4.2.2 Impact of root branching patterns

After the rhizodeposits are released at the root tip or in a small zone behind the root tip, they gradually diffuse and are decomposed by microorganisms. The number of root tips, which is related to the branching density of a root system, therefore has a significant impact on the total mass of released rhizodeposits, but also on the soil volume with rhizodeposit concentrations above the threshold value. Fig. 4 shows the rhizodeposition patterns around two simple herringbone root systems with different branching densities for both citrate and mucilage. An increase in branching density by a factor of two (from 9 to 16 root tips) increased the total mass of rhizodeposits present in the soil domain by 48 % for citrate and by 79 % for mucilage after 10 days of growth. This difference is caused by the differences in rhizodeposit release, diffusion, decomposition and sorption rate between citrate and mucilage. It can be seen that there are no rhziodeposit hotspot volumes (depicted in pink) around the upper laterals. This is because root growth and therefore also rhizodeposit release of lateral roots has already stopped and the ongoing decomposition and diffusion processes have led

to rhizodeposit concentrations below the threshold value. It can also be seen that the citrate rhizodeposit hotspot volumes are located further behind the root apex than the mucilage rhizodeposit hotspot volumes. This difference is caused by the differences in the deposition lengths (Table 1 and cf. Fig.1 (a)). An increase in branching density by a factor of two increased the total rhizodeposit hotspot volume by 80 % and 73 %, the length-normalized hotspot volume by 13 % and 9 % and the volume-normalized hotspot volume by 51 % and 29 % for citrate and mucilage, respectively, after 10 days of growth. For our parameterization, root branching thus had a greater impact on the total rhizodeposit hotspot volume and also on the rhizodeposition efficiency of citrate than of mucilage. If lateral branches were shorter, the opposite would have been the case due to the difference in deposition length between citrate and mucilage.

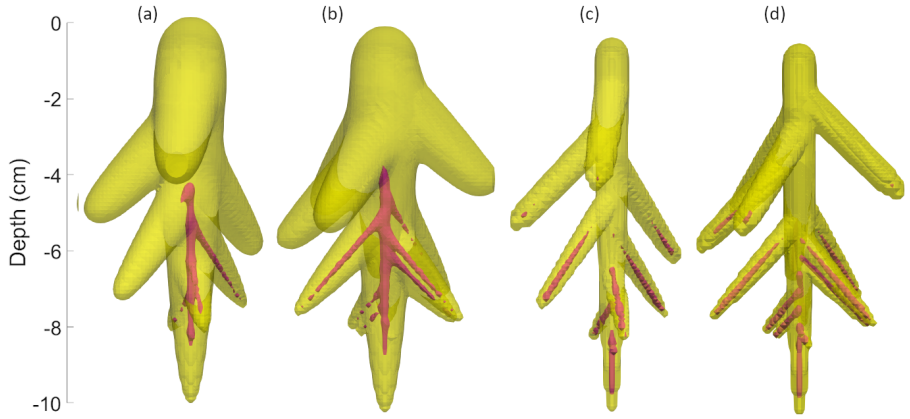

Figure 4: Deposition patterns of rhizodeposit hotspot concentrations (pink) and concentrations above the arbitrary threshold of $0.1\,\mu g\,cm^{-3}$ (yellow) for citrate (a,b) and mucilage (c,d) around a simple herringbone root system with different branching densities ($1\,cm^{-1}$ (a,c) and $2\,cm^{-1}$ (b,d)) after 10 days of growth at a constant growth rate of $1\,cm\,d^{-1}$

4.3 Scenario III: Rhizodeposit concentration patterns around the root systems of *Vicia faba* and *Zea mays*

Fig. 5 shows the rhizodeposit concentration patterns of citrate and mucilage around the 21 day old root systems of *Vicia faba* and *Zea mays*. The maximum extent of the rhizosphere was defined using an arbitrary threshold of $0.1\,\mu g\,cm^{-3}$. Due to the higher deposition rates (Table 1), the maximum mucilage concentrations are larger than the maximum citrate concentrations for both *Vicia faba* and *Zea mays* and the concentrations of one specific rhizodeposit (citrate respectively mucilage) are larger for *Vicia faba* than for *Zea mays*. Furthermore, it can be seen that the extent of the citrate rhizosphere (Fig. 5

(a,c)) is larger than the extent of the mucilage rhizosphere (Fig. 5 (b,d)). This is caused by the different properties of citrate and mucilage (Table 1).

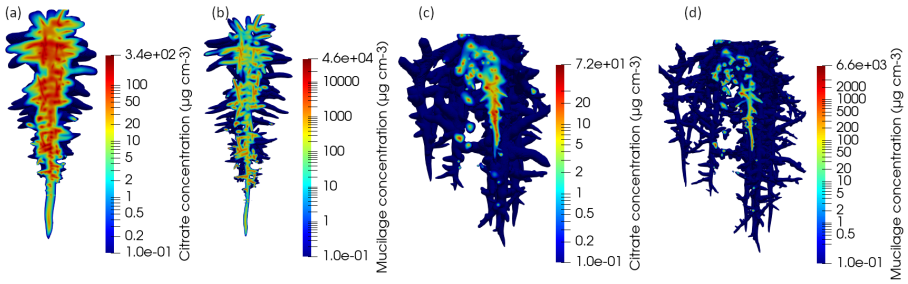

Figure 5: Vertical cut through the distribution of the rhizodeposit concentrations around 21 day old root systems (citrate around *Vicia faba* (a), mucilage around *Vicia faba* (b), citrate around *Zea mays* (c), mucilage around *Zea mays* (d)); note that the colors are in logarithmic scale and that the color scales differ for the different figures

4.3.1 Differences in the rhizodeposition patterns around the tap and fibrous root systems of *Vicia faba* and *Zea mays*

Fig. 6 shows the amount of released citrate and mucilage rhizodeposits from the root systems of *Vicia faba* and *Zea mays* with time. The total mass of rhizodeposits present in the soil domain gradually increases while the root system is growing. It is larger for mucilage than for citrate and mostly also larger for *Vicia faba* than for *Zea mays*. Only between simulation day 5 and simulation day 8, the emergence time of lateral roots of *Vicia faba*, the total rhizodeposit mass is larger for *Zea mays* than for *Vicia faba* (Fig. 6 (a)). The total mass of rhizodeposits normalized with the total root length shows very distinct patterns for *Vicia faba* and *Zea mays* (Fig. 6 (b)). For *Vicia faba*, the curve clearly reflects the development of the root architecture: At simulation day 6, the first lateral roots emerge, which is reflected by a sharp increase in the root length-normalized mucilage mass. For citrate, which is released over a length of 5 cm behind the root apex, this increase can be seen to a lesser extent and with a certain delay. For *Zea mays*, the length-normalized citrate and mucilage masses remain relatively constant over the entire simulation period, which is caused by the large number of basal roots and the early emergence of first order laterals at simulation day 3, which level out any visible impact of root architecture. Similar patterns arise for the total mass of rhizodeposits normalized with the number of root tips (Fig. 6 (c)). For *Vicia faba*, the emergence of first and second order lateral roots (simulation day 6 and 7, respectively), is reflected in the curves of both citrate and mucilage. For *Zea mays*, the curves are relatively stable over the entire simulation period. Fig. 6 (d) shows the total mass of

rhizodeposits normalized with the volume of the convex hull of the root system. At the beginning of the simulation period, the values are extremely large due to the small volume of the convex hull, but they level out at approximately simulation day 7. It can be seen that for both citrate and mucilage, the convex hull normalized rhizodeposit mass and thus the rhizodeposit concentrations are larger for *Vicia faba* than for *Zea mays*.

On simulation day 21, the root system of *Zea mays* was 2 times longer, had 3.5 times more root tips, and had a convex hull volume 3.7 times larger than the root system of *Vicia faba* (Fig. 6 (b,c,d), red curves). However, the total mass of released citrate and mucilage was only 11 % and 14 % of that of *Vicia faba*, respectively (Fig. 6 (a)). According to our simulations, the larger root system of *Zea mays* could therefore not make up for the lower rhizodeposit release rate as compared to *Vicia faba* to reach similar amounts of rhizodeposit mass released into the soil.

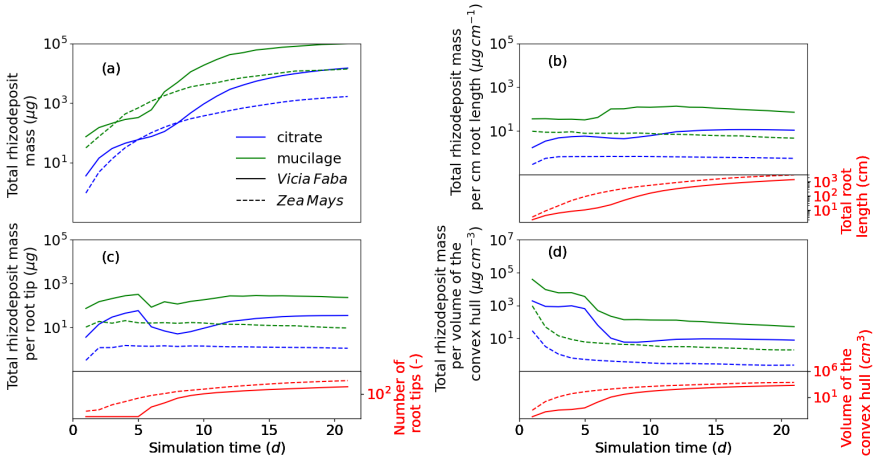

Figure 6: Total amount of released rhizodeposit mass over time (a), normalized with the total root length (b), normalized with the number of root tips (c) and normalized with the volume of the convex hull (d) for citrate and mucilage and the root systems *Vicia faba* and *Zea mays*; note that all axes are in logarithmic scale

4.3.2 Rhizodeposit hotspot analysis

Due to the steep gradients in the radial rhizodeposit concentration profiles (Fig. 1 (I b,c) and (II b,c)), only the rhizodeposit concentrations in the immediate vicinity of the root surface as well as close to growing root tips are higher than the threshold values. Due to the decomposition and diffusion processes, only the rhizodeposit concentrations around younger roots that are still growing or where rhizodeposit overlap has occurred are higher than the threshold values.

Unfortunately, the volume of rhizodeposit hotspot concentrations around the root system of *Zea mays* was so small that we could not capture it with our soil domain resolution of $1\,mm$. The hotspot analysis was therefore only performed for the root system of *Vicia faba*. An illustration of the distribution of rhizodeposit hotspots of citrate and mucilage around the root system of *Vicia faba* after 21 days of simulation is presented in Fig. 7.

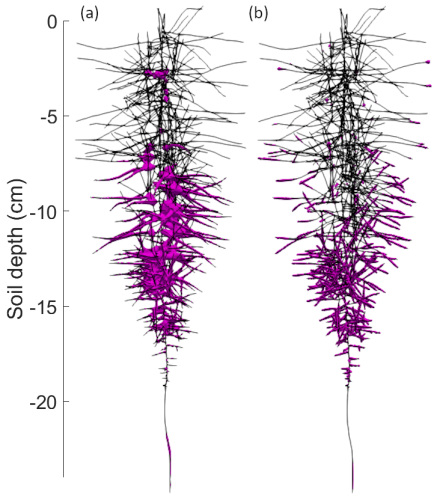

Figure 7: Distribution of rhizodeposit hotspots (pink patches) of citrate (a) and mucilage (b) around a 21 day old root system of *Vicia faba*

4.3.2.1 Development of the rhizodeposit hotspot volume and its dependence on root branching

Fig. 8 shows the development of the rhizodeposit hotspot volume and its dependence on root branching. Due to the increasing root system length and the increasing number of root tips, the rhizodeposit hotspot volume increased with increasing simulation time for both citrate and mucilage and was generally larger for citrate than for mucilage (Fig. 8 (a)). A different picture emerged, however, when the rhizodeposit hotspot volume was normalized with the root length (Fig. 8 (b)). Until simulation day 5, the root system of *Vicia faba* consisted only of a taproot without any laterals. For mucilage, which is deposited at the root tip, the root length-normalized hotspot volume therefore decreased until the emergence of lateral roots. For citrate, which is exuded over a length of $5\,cm$ behind the root apex, the root length-normalized hotspot volume increased until the deposition length was reached, and thereafter decreased until the first lateral roots emerged. At the emergence time of lateral roots, the root length-normalized hotspot volume of citrate and mucilage increased until approximately simulation day 12 and 15, respectively, and thereafter decreased. This decrease in root length normalized hotspot volume is caused on the one

hand by roots that are still growing but whose hotspot volume remains constant with growth and on the other hand by roots that have stopped growing and therefore no longer release rhizodeposits. Due to the difference in deposition length, the decrease in the root length-normalized hotspot volume occurs later for citrate than for mucilage. Fig. 8 (c) shows the development of the volume-normalized hotspot volume. Again, due to the lack of lateral roots, the volume-normalized hotspot volume decreased for both mucilage and citrate until simulation day 5. For both citrate and mucilage, it subsequently increased up to a peak value at approximately simulation day 10 and 13, respectively, and thereafter decreased again. Thus, the maximum rhizodeposition efficiency for citrate was reached on simulation day 10 and for mucilage on simulation day 13. Interestingly, until about simulation day 15, the rhizodeposition efficiency was greater for mucilage than for citrate, but about the same at the end of the simulation. This is due to the differences in rhizodeposition, diffusion, sorption and decomposition rates between citrate and mucilage.

Fig. 8 also shows the enormous effect of root branching on the development of rhizodeposit hotspots. The larger the root system became, the more important the lateral roots were for the development of the rhizodeposit hotspot volumes. At the last day of the simulation, 1^{st} order lateral roots accounted for 39% and 47% of the total rhizodeposit hotspot volume for citrate and mucilage, respectively. 2^{nd} order lateral roots accounted for 61% and 53% of the total rhizodeposit hotspot volume for citrate and mucilage and were therefore even more important than 1^{st} order lateral roots and more important for citrate than for mucilage hotspots (Fig. 8 (a)). For both citrate and mucilage, the length-normalized hotspot volume was relatively similar for lateral roots of 1^{st} and 2^{nd} order and significantly smaller for the taproot (Fig. 8 (b)). This is partly due to the shorter lateral roots compared to the taproot and partly because most of the rhizodeposits around the taproot are already decomposed at the end of the simulation. In terms of volume-normalized rhizodeposit hotspot volume, and thus rhizodeposition efficiency, the influence of 1^{st} and 2^{nd} order lateral roots was again quite similar and much smaller for the taproot. This was true for both citrate and mucilage.

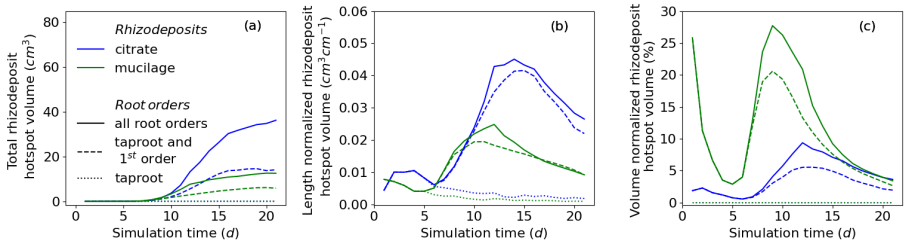

Figure 8: Impact of different root orders on the total rhizodeposit hotspot volume (a) on the total rhizodeposit hotspot volume per cm root length (b) and on the total rhizodeposit hotspot volume relative to the minimum rhizodeposit concentration volume of 99 % of the total rhizodeposit mass that is currently present in the soil domain (c)

4.3.2.2 Impact of rhizodeposit overlap on the rhizodeposit hotspot volume

Fig. 9 (a) shows the impact of overlapping rhizodeposition zones on the rhizodeposit hotspot volume of citrate and mucilage around the root system of *Vicia faba*. Interestingly, the impact of overlapping rhizodeposition zones on the total rhizodeposit hotspot volume is much more important for citrate than for mucilage. This is caused by the different rhizodeposition behaviour of citrate and mucilage: While mucilage rhizodeposition takes place exclusively at the root tip, citrate is exuded over a length of approximately 5 cm behind the root apex (Table 1). Therefore, at root branching zones, where rhizodeposition zones overlap, citrate concentrations around the individual roots are high enough to jointly produce rhizodeposit hotspots, whereas this is not the case for mucilage. Furthermore, rhizodeposit concentration volumes around the root are larger for citrate than for mucilage. The possibility of overlapping rhizodeposition zones is then also larger for citrate than for mucilage. Due to the increasing number of laterals, the relative share of total hotspot volume caused by rhizodeposit overlap increases with increasing simulation time. At simulation day 21, overlapping rhizodeposition zones accounted for 64% of the total citrate rhizodeposit hotspot volume and for 10% of the total mucilage rhizodeposit hotspot volume around the root system of *Vicia faba*. Interestingly, the total rhizodeposit hotspot volume without overlap is only slightly higher for citrate than for mucilage. In the case of high branching densities, it can be assumed that individual hotspot volumes around roots will overlap, thereby leading to a decrease in the total rhizodeposit hotspot volume. For our parameterization, however, the hotspot volumes that were created by rhizodeposition overlap were more important than the hotspot volumes that were lost by rhizodeposition overlap. Fig. 9 (b,c) shows the location of overlapping rhizodeposition zones around the root system of *Vicia faba* on the last day of simulation. It can be seen that most of the overlap happens close to the root axis where the branching takes place.

Rhizodeposit overlap due to individual roots that cross each other freely in the soil domain is less significant.

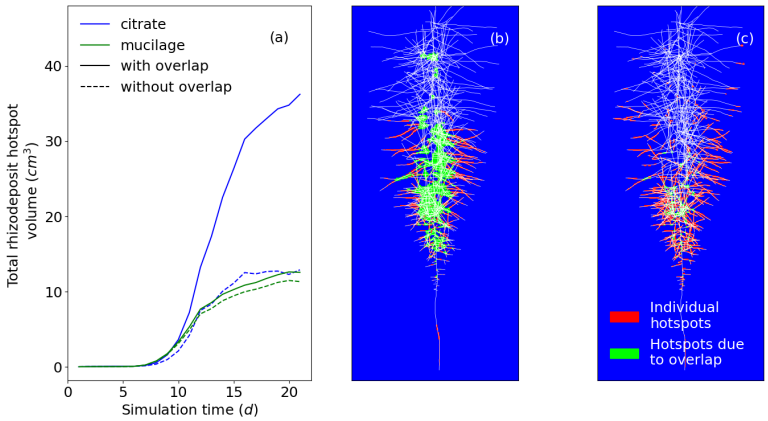

Figure 9: Impact of overlapping rhizodeposition zones on the total rhizodeposit hotspot volume (a), maximal projection along the y-axis of the location of rhizodeposit hotspots caused by overlapping rhizodeposition zones and caused by rhizodeposition from individual roots for citrate (b) and mucilage (c) on simulation day 21

4.3.2.3 Analysis of the duration of rhizodeposit hotspots

The maximum number of days on which hotspot concentrations were reached at a specific location in the soil domain was 16 days for citrate and 9 days for mucilage (Fig. 10 (a)). In general, the longer the duration of the hotspots, the lower was the volume of rhizodeposit hotspots and thus the frequency of rhizodeposit hotspot duration. Interestingly, the most common duration of the rhizodeposit hotspot for mucilage was 3 days. This is the average time between the release of the mucilage at the root tip and its degradation to a concentration below the threshold value. Fig. 10 (b, c) shows the local distribution of the durations of the rhizodeposit hotspots. It can be seen that for both citrate and mucilage, the longest duration of rhizodeposit hotspots occurs near the taproot, where root branching takes place and therefore overlapping rhizodeposit zones occur more frequently. Furthermore, long-lasting rhizodeposit hotspots occur more frequently around older parts of the root system. Lateral roots of higher order at a greater distance from the taproot do not show long durations of rhizodeposit hotspots. This effect is more pronounced for citrate than for mucilage.

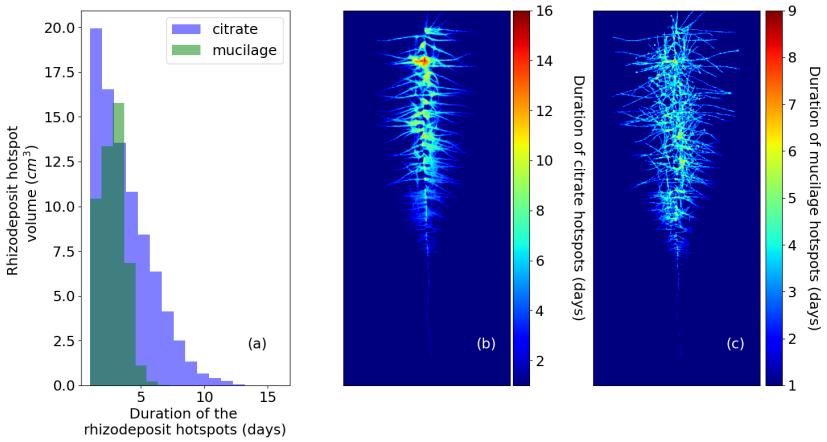

Figure 10: Duration and volume of rhizodeposit hotspots for citrate and mucilage (a); maximal projection along the y-axis of the duration of rhizodeposit hotspots at the different locations in the soil domain for citrate (b) and mucilage (c)

4.3.2.4 Analysis of distance maps from rhizodeposit hotspots

Histograms of distance maps (Fig. 11) of *Vicia faba* show that the volume of soil that is close to a hotspot increases more and more over the simulated 20 day period. At day 5, the small root system and its hotspots are in the top center of the pot and the equidistant surfaces with distances of less than 10 cm from the hotspots are approximately semi-spheres around the root system: the parabolic increase of the histogram for less than 10 cm distances corresponds to the increase in area of a semi-sphere of radius r which is $0.5 \cdot (4\pi r^2)$. At a distance of around 10 - 15 cm, which corresponds to the phase where the equidistant surface reaches the side boundaries of the pot, the histogram line decreases. From 15 - 35 cm it remains rather constant and then drops rapidly at a distance of 35 cm, which corresponds to the phase where the equidistant surface reaches the lower boundary of the pot. At day 10, more and deeper hostspots have emerged and as a consequence the peak in the histogram at around 10 cm becomes smoother and the drop of the curve occurs now already at 25 cm. At day 15, the heterogeneous distribution of several hotspots within the domain results in a rough histogram line for distances of less than 10 cm and hotspots in deeper regions cause a drop at already 15 - 20 cm distance where the equidistant surface reaches the lower boundary of the pot. Till day 15, the curves for citrate and mucilage are very similar. At day 20, for citrate, there is a peak of the soil volume at a distance of 5 cm from the hotspots and for mucilage at a distance of 3 cm. At day 20, mucilage shows a larger soil volume

in the first five centimeters compared to citrate, which is caused by the wider respectively less clumped distribution of the mucilage hotspots (cf. Fig. 7).

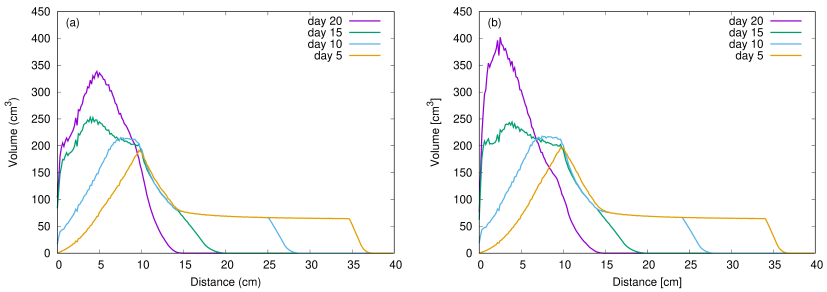

Figure 11: Histograms of distance maps of the Euclidean 3D distance from nearest citrate (a) and mucilage (b) hotspots for *Vicia faba* at day 5, day 10, day 15 and day 20; note that the scales differ in the sub-figures (a) and (b)

5 Discussion

5.1 The rhizodeposition model

In our rhizodeposition model, the roots are considered as line sources. The potential impact of the root diameter on the concentration of rhizodeposits is therefore neglected. To fulfill this assumption, the used grid resolution must be larger than the root diameter. On the other hand, a fine enough grid resolution must be chosen to capture small-scale variations in the spatial distribution of rhizodeposits caused by the steep gradients. Considering that primary roots of *Vicia faba* and *Zea mays* have mean root diameters of approximately $0.95\,mm$ and $0.85\,mm$ (Materechera et al., 1991), we assumed that a grid resolution of $1\,mm$ is suitable to simulate the spatio-temporal distribution of rhizodeposits around the growing root systems of *Vicia faba* and *Zea mays*.

For a soil domain with dimensions of $40 \times 40 \times 35\,cm$, this resolution resulted in a total number of 5.6×10^7 grid points. For each of these grid points, the rhizodeposit concentration had to be calculated analytically. To keep computation times within acceptable limits, we computed the rhizodeposit concentrations only within a specified radius around each root and parallelized the computation of rhizodeposit concentrations around individual roots.

To overcome the problem of the line source assumption as well as the high computational cost, the analytical solution could be transformed into a numerical approach. Such a numerical approach could also be integrated into a 3D multi-component model of solute transport in soil and roots like the one proposed by Mai et al. (2019). This model could then be used to study nutrient acquisition by the root system under the influence of dynamic rhizodeposition patterns and furthermore to evaluate the impact of root hairs respectively differences in root diameter on rhizodeposition patterns.

In all simulations, we assumed a constant water content of $0.3\,cm^3\,cm^{-3}$ in the rhizosphere over the entire simulation period. This assumption is supported by the experimental work of Holz et al. (2018b) and Moradi et al. (2011), who found that the water content in the rhizosphere remained constant regardless of drought stress, which they explained with the high water holding capacity of the mucilage present in the rhizosphere.

In our rhizodeposition model, we did not consider the effect of root hairs. Holz et al. (2018b) showed that plants with root hairs released significantly more carbon into the soil than plants without root hairs. Carminati et al. (2016b) suggested that the interaction between root hairs and mucilage may have an important influence on root water uptake. While the role of root hairs is to extend the functional root radius (Segal et al., 2008), mucilage may keep the rhizosphere and the space between root hairs moist, thereby facilitating water flow into root hairs under negative soil water potentials. As a further development, it would thus be interesting to extend our rhizodeposition model by the function of root hairs.

To date, it is not clear how the release of rhizodeposits from an individual root develops with root aging. In our model, we assumed a constant rhizodeposition release rate while the root is growing. As soon as the root stops growing, also rhizodeposition is assumed to stop. Several experimental studies have reported that the total mass of rhizodeposits around a root root system is low at the seedling stage of a plant, increases until flowering, and then decreases at maturity (Aulakh et al., 2001; Gransee and Wittenmayer, 2000; Krasil'nikov et al., 1958; Nguyen, 2009). Our model assumptions allow us to simulate such rhizodeposition behaviour and we therefore consider them as justified.

Fresh mucilage, which is in contact with water, is known to diffuse freely into the soil (Sealey et al., 1995). When the soil dries, however, mucilage forms strong bonds between soil particles and can no longer move by diffusive transport (Ahmed et al., 2014; Albalasmeh and Ghezzehei, 2014; Sealey et al., 1995). In our simulations, we assumed a constant soil water content and did not take into account soil drying. Mucilage was therefore also assumed to diffuse freely into the soil. In simulations where soil drying is considered, however, the immobilization of mucilage must be taken into account.

When microbes decompose mucilage, they are known to simultaneously release gel-like substances called bacterial exopolysaccharides (EPS) (Carminati and Vetterlein, 2013). It has been shown that these substances have similar physical properties to mucilage and are therefore likely to have an effect on the hydraulic properties of the soil (Or et al., 2007). In our study, simulated concentrations of mucilage only refer to fresh mucilage, but not to mucilage derivatives. Similarly, we only considered concentrations of fresh mucilage above the specified threshold value as mucilage hotspots. However, for simulations in which both mucilage deposition and soil water transport are taken into account, the impact of mucilage derivatives on soil hydraulic properties must be considered.

5.2 Rhizodeposition by a single growing root

The simulated radial extent of citrate and mucilage rhizodeposit hotspot rhizospheres was $1\,mm$ and $0.5\,mm$, respectively. The simulated radial extent of citrate and mucilage rhizopheres in which the rhizodeposit concentration was below the threshold value, but still detectable, was $4-9\,mm$ and $2-5\,mm$, respectively. For mucilage, these values are in the same range as the experimental findings by Holz et al. (2018a) and the calculated values by Zickenrott et al. (2016), who reported rhizosphere extents between $0.6\,mm$ and $2\,mm$. For citrate, the radial rhizosphere extents are in the same order of magnitude as the results for rhizodeposited ^{14}C by Kuzyakov et al. (2003), who measured a zone of maximum carbon exudate concentration within a distance of $1-2\,mm$ from the root surface and a zone of less significant amounts of carbon exudate concentration within a distance of $3-10\,mm$ from the root surface. It must be noted that the experimental conditions and model assumptions in the studies by Holz et al. (2018a), Zickenrott et al. (2016) and Kuzyakov et al. (2003) were not the same as in our modelling setup. They differed with regard to plant species, plant age, water content and pot geometry and may therefore only be regarded as an indicative of the order of magnitude.

5.3 Impact of root architectural traits on rhizodeposition patterns

It is well known that root architectural traits have a significant effect on the distribution of rhizodeposits around the root system and thus on rhizosphere processes (Holz et al., 2018b; Lynch, 1995; Nielsen et al., 1994). A detailed analysis about the impact of individual root architectural traits such as root growth rate and branching density on rhizodeposit hotspot volumes and on the rhizodeposition efficiency, however, is still lacking.

Holz et al. (2018b) suggested that reduced root elongation leads to a higher rhizodeposit concentration per rhizosphere soil volume and thus - in the case of mucilage - to an increase in the local water content. In the present study, we made a more detailed analysis of the impact of different root growth rates on the rhizodeposit concentration per rhizosphere soil volume. Considering that a minimum rhizodeposit concentration is required to trigger certain processes, such as an increase in soil water content in the case of mucilage or increased phosphorus mobilization in the case of citrate, an intermediate root growth rate has the greatest effect on rhizosphere processes. If root growth is too fast, the soil volume containing rhizodeposits is large, but the rhizodeposit concentration is below the threshold that triggers a specific rhizosphere process. If root growth is too low, the rhizodeposit concentration is very high, but the soil volume containing such high rhizodeposit concentrations is very low. For our parameterization, the optimal growth rate has been shown to be greater for mucilage than for citrate. It can be speculated that roots take advantage of this effect: When root elongation decreases due to environmental factors, such as soil mechanical impedance, a larger rhizodeposit hotspot volume may result in

increased rhizosphere water content in the case of mucilage or increased phosphate availability in the case of citrate, thus compensating for the disadvantages of a smaller root system.

Nielsen et al. (1994) and Lynch (1995) reported that highly branched root systems with a large number of root tips have a higher nutrient uptake efficiency and thus a greater influence on rhizosphere processes. Similarly, (Fletcher et al., 2020) found that the number of root tips of a root system correlated well with an increase in citrate-enhanced phosphate uptake. This is consistent with the results of our simulations, which also showed larger soil volumes of rhizodeposit hotspots when the number of root tips was increased.

5.4 Rhizodeposition patterns around growing root systems

Zickenrott et al. (2016) estimated that mucilage concentrations of up to $4 \times 10^4\,\mu g\,cm^{-3}$ soil can potentially occur in the rhizosphere. In our simulations, the maximum observed mucilage concentrations ranged between $6.6 \times 10^3\,\mu g\,cm^{-3}$ soil for *Zea mays* and $2.7 \times 10^5\,\mu g\,cm^{-3}$ soil for *Vicia faba* and are therefore in good agreement with this estimated maximum value. Gerke (2015) and Jones (1998) found maximum citrate concentrations in the rhizosphere between 1×10^3 and $4 \times 10^3\,\mu g\,cm^{-3}$ soil. These ranges are a bit higher than our maximum simulated citrate concentrations of $72\,\mu g\,cm^{-3}$ soil for *Zea mays* and $938\,\mu g\,cm^{-3}$ soil for *Vicia faba*. This can be explained by the fact that other plants such as *Lupinus albus* and *Cicer arietinum* have been shown to release much greater amounts of citrate into the soil than *Vicia faba* and, even more significantly, than *Zea mays* (Lyu et al., 2016).

It is well known that fibrous root systems such as *Zea mays* show lower rhizodeposit release rates than tap root systems such as *Vicia faba* (Lyu et al., 2016; Zickenrott et al., 2016). On the other hand, fibrous root systems generally have a much larger number of root tips, from which rhizodeposits are released. Our hypothesis was that the greater number of root tips of *Zea mays* may compensate for the lower rhizodeposit release rates, producing similar amounts of mucilage and citrate release into the soil as the tap root system *Vicia faba*. This hypothesis, however, could not be confirmed. Even though the simulated root system of *Zea mays* was 2 times longer and had 3.5 times more root tips than the simulated root system of *Vicia faba* on the last day of simulation, the total simulated mass of released rhizodeposits around the root system of *Zea mays* relative to *Vicia faba* was only 21 % for mucilage and 11 % for citrate. These results indicate that *Zea mays* and *Vicia faba* employ different strategies in the interplay between root morphological and root physiological traits to optimize root water and nutrient acquisition.

The rhizodeposit hotspot analysis showed the importance of root branching and the role of overlapping rhizodeposition zones for the development of rhizodeposit hotspots. 1^{st} and 2^{nd} order lateral roots accounted for approximately 40 % and 60 % of the total rhizodeposit hotspot volume around a 21 day old root system of *Vicia faba*. This was true for both citrate and mucilage. In contrast,

the influence of rhizodeposit overlap on the total rhizodeposit hotspot volume was found to be quite different for citrate and mucilage: while rhizodeposit overlap accounted for 64 % of the total rhizodeposit hotspot volume of citrate, it was responsible for only 10 % of the total rhizodeposit hotspot volume of mucilage after 21 days of simulation. These differences are caused primarily by differences in the rhizodeposit release: while mucilage is deposited exclusively at the root tip, citrate release takes place over a length of approximately 5 cm behind the root tip. Additionally, due to the larger diffusion coefficient of citrate compared to mucilage, rhizodeposit concentration volumes around individual roots are larger for citrate than for mucilage and the possibility of rhizodeposit overlap is thus also greater for citrate than for mucilage. It must be noted that we only looked at a single root system in the present study. If multiple neighbouring root systems were considered, the impact of overlapping rhizodeposition zones on the total rhizodeposit hotspot volume would be even larger.

Our rhizodeposit hotspot analysis showed that rhizodeposit concentrations were above the defined thresholds only in the immediate vicinity of the root surface near root tips or near root branching zones. Around the root system of *Zea mays*, which has a lower rhizodeposit release rate per root tip than *Vicia faba*, rhizodeposit hotspot volumes of both citrate and mucilage were generally too small to be captured by our simulation model. Similar results were reported by Fletcher et al. (2019) and Fletcher et al. (2020) for citrate, who have shown in modelling studies that the critical concentration threshold around a root leading to enhanced phosphorus mobilization is hardly ever reached.

There are numerous modeling studies in the literature on root foraging strategies that use 3D root architecture models (e.g. Ge et al. (2000), Lynch (1995), and Pagès (2011)). However, all of these studies concentrated on the analysis of nutrient depletion zone overlap and did not consider the impact of overlapping rhizodeposition zones on nutrient supply. De Parseval et al. (2017) used a 2D model approach to investigate the interaction between inter-root competition and inter-root facilitation in the horizontal plane. Inter-root competition is caused by the overlap of nutrient depletion zones, while inter-root facilitation is based on the overlap of rhizodeposition zones, which leads to rhizodeposit hotspots and consequently to an increased nutrient availability. Based on the distances between roots, this model approach allowed them to predict whether competition, facilitation or no interaction is the predominant process governing root phosphorus uptake. It would be pertinent to use our model to bridge these studies and to extend previous modelling approaches on root foraging strategies by the aspect of inter-root facilitation. This would give us a more realistic estimate about the impact of root architecture on root nutrient uptake.

5.5 Conclusion

In this study, we presented a new model to simulate the spatiotemporal distribution patterns of rhizodeposits around growing root systems in three dimensions. The novel model approach allowed us to evaluate the effects of root architecture

features such as root growth rate and branching density on the development of rhizodeposit hotspot zones, which can trigger specific rhizosphere processes such as increased nutrient uptake by roots. It further enabled the investigation of the influence of differences in rhizodeposit properties and root architectures of different plant species on rhizodeposition patterns. We could show that rhizodeposit hotspot volumes around roots were at a maximum at intermediate root growth rates and that branching allowed the rhizospheres of individual roots to overlap, resulting in an increase in the volume of rhizodeposit hotspot zones. We could also show that the volume of rhizodeposit hotspots was smaller around the fibrous root system *Zea mays* than around the tap root system *Vicia faba*.

Further work includes the integration of our model into a 3D multi-component root and solute transport model (Mai et al., 2019). This model can then be used to mechanistically explain experimentally observed rhizodeposition patterns (e.g., using zymography or $^{11}CO_2$-labeling (Giles et al., 2018; Yin et al., 2020)). We also aim to incorporate the influence of root hairs and root diameters into our model to gain a better understanding of the water and nutrient acquisition strategies of different plant species.

5.6 Acknowledgements

This project was carried out in the framework of the priority program 2089 'Rhizosphere spatiotemporal organization – a key to rhizosphere functions' funded by the German Research Foundation DFG under the project number 403641034. A.H. and E.K. have been funded by the German Research Foundation DFG under Germany's Excellence Strategy – EXC 2070 – 390732324.

References

Ahmed, M. A., Kroener, E., Holz, M., Zarebanadkouki, M., & Carminati, A. (2014). Mucilage exudation facilitates root water uptake in dry soils. *Functional Plant Biology*, *41*(11), 1129–1137. https://doi.org/10.1071/FP13330

Ahmed, M. A., Kroener, E., Benard, P., Zarebanadkouki, M., Kaestner, A., & Carminati, A. (2016). Drying of mucilage causes water repellency in the rhizosphere of maize: Measurements and modelling. *Plant and Soil*, *407*(1-2), 161–171. https://doi.org/10.1007/s11104-015-2749-1

Albalasmeh, A. A., & Ghezzehei, T. A. (2014). Interplay between soil drying and root exudation in rhizosheath development. *Plant and Soil*, *374*(1-2), 739–751. https://doi.org/10.1007/s11104-013-1910-y

Aulakh, M., Wassmann, R., Bueno, C., Kreuzwieser, J., & Rennenberg, H. (2001). Characterization of root exudates at different growth stages of ten rice (oryza sativa l.) cultivars. *Plant biology*, *3*(2), 139–148. https://doi.org/10.1055/s-2001-12905

Bear, J., & Cheng, A. H.-D. (2010). *Modeling groundwater flow and contaminant transport* (Vol. 23). Springer Science & Business Media.

Benard, P., Zarebanadkouki, M., Brax, M., Kaltenbach, R., Jerjen, I., Marone, F., Couradeau, E., Felde, V. J., Kaestner, A., & Carminati, A. (2019). Microhydrological niches in soils: How mucilage and eps alter the biophysical properties of the rhizosphere and other biological hotspots. *Vadose Zone Journal*, *18*(1), 1–10. https://doi.org/10.2136/vzj2018.12.0211

Carminati, A., Kroener, E., Ahmed, M. A., Zarebanadkouki, M., Holz, M., & Ghezzehei, T. (2016a). Water for carbon, carbon for water. *Vadose Zone Journal*, *15*(2), 1–10. https://doi.org/10.2136/vzj2015.04.0060

Carminati, A., & Vetterlein, D. (2013). Plasticity of rhizosphere hydraulic properties as a key for efficient utilization of scarce resources. *Annals of botany*, *112*(2), 277–290. https://doi.org/10.1093/aob/mcs262

Carminati, A., Zarebanadkouki, M., Kroener, E., Ahmed, M. A., & Holz, M. (2016b). Biophysical rhizosphere processes affecting root water uptake. *Annals of Botany*, *118*(4), 561–571. https://doi.org/10.1093/aob/mcw113

Carslaw, H., & Jaeger, J. (1959). *Conduction of heat in solids*. Clarendon Press. https://doi.org/10.1007/978-3-319-48090-9_9

Carson, J. K., Gonzalez-Quiñones, V., Murphy, D. V., Hinz, C., Shaw, J. A., & Gleeson, D. B. (2010). Low pore connectivity increases bacterial diversity in soil. *Applied and environmental microbiology*, *76*(12), 3936–3942. https://doi.org/10.1128/AEM.03085-09

Cheng, W., & Gershenson, A. (2007). Carbon fluxes in the rhizosphere. *The rhizosphere* (pp. 31–56). Elsevier. https://doi.org/0.1016/B978-012088775-0/50004-5

Crank, J. (1979). *The mathematics of diffusion*. Oxford university press.

Darrah, P. (1991). Models of the rhizosphere. *Plant and Soil*, *133*(2), 187–199.

De Parseval, H., Barot, S., Gignoux, J., Lata, J.-C., & Raynaud, X. (2017). Modelling facilitation or competition within a root system: Importance of the overlap of root depletion and accumulation zones. *Plant and soil*, *419*(1-2), 97–111. https://doi.org/10.1007/s11104-017-3321-y

Evans, L. C. (1998). Partial differential equations. *Graduate studies in mathematics*, *19*(2).

Fletcher, D. M., Ruiz, S., Dias, T., Petroselli, C., & Roose, T. (2020). Linking root structure to functionality: The impact of root system architecture on citrate-enhanced phosphate uptake. *New Phytologist*, *227*(2), 376–391. https://doi.org/doi.org/10.1111/nph.16554

Fletcher, D. M., Shaw, R., Sánchez-Rodrıguez, A., Daly, K., Van Veelen, A., Jones, D., & Roose, T. (2019). Quantifying citrate-enhanced phosphate root uptake using microdialysis. *Plant and Soil*, 1–21. https://doi.org/10.1007/s11104-019-04376-4

Gao, W., Blaser, S. R., Schlüter, S., Shen, J., & Vetterlein, D. (2019). Effect of localised phosphorus application on root growth and soil nutrient dynamics in situ–comparison of maize (zea mays) and faba bean (vicia faba) at the seedling stage. *Plant and Soil*, *441*(1-2), 469–483. https://doi.org/10.1007/s11104-019-04138-2

Ge, Z., Rubio, G., & Lynch, J. P. (2000). The importance of root gravitropism for inter-root competition and phosphorus acquisition efficiency: Results from a geometric simulation model. *Plant and soil*, *218*(1-2), 159–171. https://doi.org/10.1023/A:1014987710937

Gerke, J. (2015). The acquisition of phosphate by higher plants: Effect of carboxylate release by the roots. a critical review. *Journal of Plant Nutrition and Soil Science*, *178*(3), 351–364. https://doi.org/10.1002/jpln.201400590

Giles, C., Dupuy, L., Boitt, G., Brown, L., Condron, L., Darch, T., Blackwell, M., Menezes-Blackburn, D., Shand, C., Stutter, M., et al. (2018). Root development impacts on the distribution of phosphatase activity: Improvements in quantification using soil zymography. *Soil Biology and Biochemistry*, *116*, 158–166. https://doi.org/10.1016/j.soilbio.2017.08.011

Gransee, A., & Wittenmayer, L. (2000). Qualitative and quantitative analysis of water-soluble root exudates in relation to plant species and development. *Journal of plant nutrition and soil science*, *163*(4), 381–385. https://doi.org/10.1002/1522-2624(200008)163:4⟨381::AID-JPLN381⟩3.0.CO;2-7

Hinsinger, P., Bengough, A. G., Vetterlein, D., & Young, I. M. (2009). Rhizosphere: Biophysics, biogeochemistry and ecological relevance. *Plant and soil*, *321*(1-2), 117–152. https://doi.org/10.1007/s11104-008-9885-9

Hodge, A., Berta, G., Doussan, C., Merchan, F., & Crespi, M. (2009). Plant root growth, architecture and function. *Plant and soil*, *321*(1-2), 153–187. https://doi.org/10.1007/s11104-009-9929-9

Holz, M., Leue, M., Ahmed, M. A., Benard, P., Gerke, H. H., & Carminati, A. (2018a). Spatial distribution of mucilage in the rhizosphere measured with infrared spectroscopy. *Frontiers in Environmental Science*, *6*, 87. https://doi.org/10.3389/fenvs.2018.00087

Holz, M., Zarebanadkouki, M., Kaestner, A., Kuzyakov, Y., & Carminati, A. (2018b). Rhizodeposition under drought is controlled by root growth rate and rhizosphere water content. *Plant and soil*, *423*(1-2), 429–442. https://doi.org/10.1007/s11104-017-3522-4

Iijima, M., Sako, Y., & Rao, T. (2003). A new approach for the quantification of root-cap mucilage exudation in the soil. *Roots: The dynamic interface between plants and the earth* (pp. 399–407). Springer. https://doi.org/10.1023/A:1026183109329

Jacques, D., Šimnek, J., Mallants, D., & Van Genuchten, M. T. (2018). The hpx software for multicomponent reactive transport during variably-saturated flow: Recent developments and applications. *Journal of Hydrology and Hydromechanics*, *66*(2), 211–226. https://doi.org/10.1515/johh-2017-0049

Jones, D. L. (1998). Organic acids in the rhizosphere–a critical review. *Plant and soil*, *205*(1), 25–44. https://doi.org/10.1023/A:1004356007312

Kirk, G. D. (1999). A model of phosphate solubilization by organic anion excretion from plant roots. *European Journal of Soil Science*, *50*(3), 369–378. https://doi.org/10.1111/j.1365-2389.1999.00239.x

Krasil'nikov, N. et al. (1958). Soil microorganisms and higher plants. *Soil microorganisms and higher plants.*

Kuzyakov, Y., Raskatov, A., & Kaupenjohann, M. (2003). Turnover and distribution of root exudates of zea mays. *Plant and Soil*, *254*(2), 317–327. https://doi.org/10.1023/A:1025515708093

Lobet, G., Pound, M. P., Diener, J., Pradal, C., Draye, X., Godin, C., Javaux, M., Leitner, D., Meunier, F., Nacry, P., et al. (2015). Root system markup language: Toward a unified root architecture description language. *Plant Physiology*, *167*(3), 617–627. https://doi.org/10.1104/pp.114.253625

Lynch, J. (1995). Root architecture and plant productivity. *Plant physiology*, *109*(1), 7. https://doi.org/10.1104/pp.109.1.7

Lynch, J. P., Ho, M. D. et al. (2005). Rhizoeconomics: Carbon costs of phosphorus acquisition. *Plant and soil*, *269*(1-2), 45–56. https://doi.org/10.1007/s11104-004-1096-4

Lyu, Y., Tang, H., Li, H., Zhang, F., Rengel, Z., Whalley, W. R., & Shen, J. (2016). Major crop species show differential balance between root morphological and physiological responses to variable phosphorus supply. *Frontiers in Plant Science*, *7*, 1939. https://doi.org/10.3389/fpls.2016.01939

Mai, T. H., Schnepf, A., Vereecken, H., & Vanderborght, J. (2019). Continuum multiscale model of root water and nutrient uptake from soil with explicit consideration of the 3d root architecture and the rhizosphere gradients. *Plant and Soil*, *439*(1-2), 273–292. https://doi.org/10.1007/s11104-018-3890-4

Manschadi, A. M., Kaul, H.-P., Vollmann, J., Eitzinger, J., & Wenzel, W. (2014). Developing phosphorus-efficient crop varieties—an interdisciplinary research framework. *Field Crops Research*, *162*, 87–98. https://doi.org/10.1016/j.fcr.2013.12.016

Materechera, S., Dexter, A., & Alston, A. M. (1991). Penetration of very strong soils by seedling roots of different plant species. *Plant and soil*, *135*(1), 31–41. https://doi.org/10.1007/BF00014776

Moradi, A. B., Carminati, A., Vetterlein, D., Vontobel, P., Lehmann, E., Weller, U., Hopmans, J. W., Vogel, H.-J., & Oswald, S. E. (2011). Three-dimensional visualization and quantification of water content in the rhizosphere. *New Phytologist*, *192*(3), 653–663. https://doi.org/10.1111/j.1469-8137.2011.03826.x

Nguyen, C. (2009). Rhizodeposition of organic c by plant: Mechanisms and controls. *Sustainable agriculture* (pp. 97–123). Springer. https://doi.org/10.1007/978-90-481-2666-8_9

Nguyen, C., Froux, F., Recous, S., Morvan, T., & Robin, C. (2008). Net n immobilisation during the biodegradation of mucilage in soil as affected by

repeated mineral and organic fertilisation. *Nutrient Cycling in Agroecosystems*, *80*(1), 39–47. https://doi.org/10.1007/s10705-007-9119-1

Nielsen, K. L., Lynch, J. P., Jablokow, A. G., & Curtis, P. S. (1994). Carbon cost of root systems: An architectural approach. *Plant and Soil*, *165*(1), 161–169. https://doi.org/10.1007/BF00009972

Nye, P. (1966). The effect of the nutrient intensity and buffering power of a soil, and the absorbing power, size and root hairs of a root, on nutrient absorption by diffusion. *Plant and Soil*, *25*(1), 81–105. https://doi.org/10.1007/BF01347964

Oburger, E., Jones, D. L., & Wenzel, W. W. (2011). Phosphorus saturation and ph differentially regulate the efficiency of organic acid anion-mediated p solubilization mechanisms in soil. *Plant and Soil*, *341*(1-2), 363–382. https://doi.org/10.1007/s11104-010-0650-5

Olesen, T., Moldrup, P., Yamaguchi, T., & Rolston, D. (2001). Constant slope impedance factor model for predicting the solute diffusion coefficient in unsaturated soil. *Soil Science*, *166*(2), 89–96. https://doi.org/10.1097/00010694-200102000-00002

Ollion, J., Cochennec, J., Loll, F., Escudé, C., & Boudier, T. (2013). Tango: A generic tool for high-throughput 3d image analysis for studying nuclear organization. *Bioinformatics*, *29*(14), 1840–1841. https://doi.org/10.1093/bioinformatics/btt276

Or, D., Phutane, S., & Dechesne, A. (2007). Extracellular polymeric substances affecting pore-scale hydrologic conditions for bacterial activity in unsaturated soils. *Vadose Zone Journal*, *6*(2), 298–305. https://doi.org/10.2136/vzj2006.0080

Pagès, L. (2011). Links between root developmental traits and foraging performance. *Plant, Cell & Environment*, *34*(10), 1749–1760.

Pausch, J., Tian, J., Riederer, M., & Kuzyakov, Y. (2013). Estimation of rhizodeposition at field scale: Upscaling of a 14 c labeling study. *Plant and Soil*, *364*(1-2), 273–285. https://doi.org/10.1007/s11104-012-1363-8

Pineros, M. A., Magalhaes, J. V., Alves, V. M. C., & Kochian, L. V. (2002). The physiology and biophysics of an aluminum tolerance mechanism based on root citrate exudation in maize. *Plant Physiology*, *129*(3), 1194–1206. https://doi.org/10.1104/pp.002295

Rangel, A. F., Rao, I. M., Braun, H.-P., & Horst, W. J. (2010). Aluminum resistance in common bean (phaseolus vulgaris) involves induction and maintenance of citrate exudation from root apices. *Physiologia Plantarum*, *138*(2), 176–190. https://doi.org/10.1111/j.1399-3054.2009.01303.x

Schindelin, J., Arganda-Carreras, I., Frise, E., Kaynig, V., Longair, M., Pietzsch, T., Preibisch, S., Rueden, C., Saalfeld, S., Schmid, B., et al. (2012). Fiji: An open-source platform for biological-image analysis. *Nature methods*, *9*(7), 676–682. https://doi.org/10.1038/nmeth.2019

Schnepf, A., Leitner, D., & Klepsch, S. (2012). Modeling phosphorus uptake by a growing and exuding root system. *Vadose Zone Journal*, *11*(3), vzj2012–0001. https://doi.org/10.2136/vzj2012.0001

Schnepf, A., Leitner, D., Landl, M., Lobet, G., Mai, T. H., Morandage, S., Sheng, C., Zörner, M., Vanderborght, J., & Vereecken, H. (2018). Crootbox: A structural–functional modelling framework for root systems. *Annals of botany*, *121*(5), 1033–1053. https://doi.org/10.1093/aob/mcx221

Schulz-Bohm, K., Geisen, S., Wubs, E. J., Song, C., de Boer, W., & Garbeva, P. (2017). The prey's scent–volatile organic compound mediated interactions between soil bacteria and their protist predators. *The ISME journal*, *11*(3), 817–820. https://doi.org/10.1038/ismej.2016.144

Sealey, L., McCully, M., & Canny, M. (1995). The expansion of maize root-cap mucilage during hydration. 1. kinetics. *Physiologia Plantarum*, *93*(1), 38–46. https://doi.org/10.1034/j.1399-3054.1995.930107.x

Segal, E., Kushnir, T., Mualem, Y., & Shani, U. (2008). Water uptake and hydraulics of the root hair rhizosphere. *Vadose Zone Journal*, *7*(3), 1027–1034. https://doi.org/10.2136/vzj2007.0122

Stingaciu, L., Schulz, H., Pohlmeier, A., Behnke, S., Zilken, H., Javaux, M., & Vereecken, H. (2013). In situ root system architecture extraction from magnetic resonance imaging for water uptake modeling. *Vadose zone journal*, *12*(1), 1–9. https://doi.org/10.2136/vzj2012.0019

Watt, M., Silk, W. K., & Passioura, J. B. (2006). Rates of root and organism growth, soil conditions, and temporal and spatial development of the rhizosphere. *Annals of botany*, *97*(5), 839–855. https://doi.org/10.1093/aob/mcl028

Westhoff, S., van Wezel, G. P., & Rozen, D. E. (2017). Distance-dependent danger responses in bacteria. *Current opinion in microbiology*, *36*, 95–101. https://doi.org/10.1016/j.mib.2017.02.002

Wilson, J. L., & Miller, P. J. (1978). Two-dimensional plume in uniform groundwater flow. *Journal of the Hydraulics Division*, *104*(4), 503–514. https://doi.org/10.1061/JYCEAJ.0004975

Yin, Y.-G., Suzui, N., Kurita, K., Miyoshi, Y., Unno, Y., Fujimaki, S., Nakamura, T., Shinano, T., & Kawachi, N. (2020). Visualising spatio-temporal distributions of assimilated carbon translocation and release in root systems of leguminous plants. *Scientific reports*, *10*(1), 1–11. https://doi.org/10.1038/s41598-020-65668-9

Zhou, X.-R., Schnepf, A., Vanderborght, J., Leitner, D., Lacointe, A., Vereecken, H., & Lobet, G. (2020). Cplantbox, a whole-plant modelling framework for the simulation of water-and carbon-related processes. *in silico Plants*, *2*(1), diaa001. https://doi.org/10.1093/insilicoplants/diaa001

Zickenrott, I.-M., Woche, S. K., Bachmann, J., Ahmed, M. A., & Vetterlein, D. (2016). An efficient method for the collection of root mucilage from different plant species—a case study on the effect of mucilage on soil water repellency. *Journal of Plant Nutrition and Soil Science*, *179*(2), 294–302. https://doi.org/10.1002/jpln.201500511